TOWARDS A MULTISCALE COMPUTATIONAL FRAMEWORK FOR SIMULATING FLOW MEDIATED CRYSTALLIZATION BASED ON PHASE-FIELD CRYSTAL FORMALISMS

L. CONNOR WILLIS[1], REKHA R. RAO[2] AND Z. LEONARDO LIU[1]

[1]Department of Chemical and Biomedical Engineering
FAMU-FSU College of Engineering
2525 Pottsdamer St, Tallahassee, FL 32310
Email: chemical@eng.famu.fsu.edu, Web page: https://eng.famu.fsu.edu/cbe

[2]Sandia National Laboratories
1515 Eubank Blvd SE, Albuquerque, NM 87123
Email: partnerships@sandia.gov, Web page: https://www.sandia.gov/

Key Words: Crystallization in Flow, Phase Field Crystal Method, Thin Film Coating, Hydrodynamic Coupling

Summary. We lay the foundation and framework for a multiscale approach for studying crystallization in the presence of flow by coupling the Structural Phase Field Crystal (XPFC) formalism with the Navier-Stokes equations. We discuss the numerical techniques and verify the formalism against previous attempts with the vanilla Phase Field Crystal (PFC) formalism. Moreover, with this new Hydrodynamically coupled Structural Phase Field Crystal (HXPFC) method, we discuss unreported global and local crystal microstructural transformation induced by the flow. The HXPFC method establishes a framework to predict more complex crystal structures while incorporating physics relevant to film coating flows.

1 INTRODUCTION

Crystallization during thin film coating is a process to deposit functional species that spans many industries, from manufacturing perovskite based solar cells[1], to semiconductor production[2], and additive manufacturing[3]. Ubiquitous to all crystallization processes is the need for microstructural control for the final product efficacy. Hence, computational insights into the mechanisms dictating crystal formation and morphology during thin-film coating can support process optimization leading to reduced waste, higher efficiency, and better predictability. However, because flow mediated crystallization is inherently a multi-scale process, with many relevant length and time scales, it is not trivial to model. Depending on information desired, there are many different approaches to modelling crystallization. Two of the most common being brute force molecular dynamics (MD) simulations, on the order of magnitude of Angstroms, and classical phase-field (PF) methods, *e.g.*, the Cahn-Hilliard or Allen-Cahn formalisms, on the order of magnitude of hundreds of nanometers. However, each method has its strength and weakness. MD simulations can resolve the relevant length scales, but typically struggle to simulating up to microseconds. Alternatively, classical PF methods can easily simulate the relevant time scales, but traditionally cannot resolve the internal, solid phase, crystal structure.

In the middle of length scales sit the Classical Density Functional Theory (CDFT), the Dynamical Density Functional Theory (DDFT), and the Phase Field Crystal (PFC) method. Closely resembling the Ramakrishnan and Yussouff Theory of Freezing[4] and the Marconi and Tarazona DDFT[5], the PFC Method was first introduced by Ken Elder et al. in 2002[6,7] as an intermediate scale method of gaining molecular level information on diffusive time scales. For an excellent review article, we refer the reader to Berry et al.[8]. The PFC has been very successful in recovering the Read-Shockley equation and modelling phenomena such as liquid-phase epitaxial growth[7], crystal defect analysis[9], and Kirkendall voids[10]. However, the PFC does not come without its drawbacks. First, it has generally not been parameterized and made to quantitively match a specific material, albeit with a few notable exceptions. Second, the qualitative nature of PFC is partly due to the challenge of modelling complex crystal structures[11], assumptions of equilibrium structures, and the many other approximations made during the derivation. One of the most successful approaches to remedying the issues was the introduction of the Structural Phase Field Crystal (XPFC) method by Greenwood et al.[12,13]. Instead of expanding the direct correlation function (DCF) to a fourth order term as in PFC, the authors introduced an ansatz for the DCF that allows one to modulate the crystal planes, blazing the trail for more complex structures. Alster et al. further extended the XPFC by adding a three-body correlation function, which allows for a simple representation of a general ABX_3 perovskite[11].

Although the previous successes have been monumental, the first known attempt to couple the Navier-Stokes and PFC equations can be traced back to 2011 when Praetorius and Voigt used the PFC to model colloidal suspensions[14]. The authors only used the PFC coupling to model individual particles in the flowing solvent. In a subsequent paper, the same authors used an overdamped limit for the velocity of the flowing particles to derive a similar, but alternative approach to the Navier-Stokes PFC coupling by finding an appropriate Navier-Stokes momentum term via force balance[15]. Since then, a number of works have further refined the numerical methods of the Navier-Stokes PFC method[16,17] with little focus on understanding the physics of complex microstructural transition.

To fill this gap, we propose a Hydrodynamically coupled Structural Phase Field Crystal (HXPFC) method by coupling the Navier-Stokes equations with the XPFC formalisms to set the stage for more complex flow-mediated crystallization studies. With this novel HXPFC method, we report on previously unseen microscale crystal pattern formation based on potentially novel flow-based microstructural control strategies.

2 HYDRODYNAMIC STRUCTURAL PHASE FIELD CRYSTAL MODEL (HXPFC)

2.1 HXPFC Equations

To prepare for extending the previous works to more complex crystal structures in flow, we present the XPFC equations, equations (1)-(3) below, in conjunction with the definitions presented in Table 1. Note, the momentum coupling in equation (1) is through a gradient of chemical potential mimicking a surface tension-like forcing term regulated by the order parameter[15-17]. The DCF and the model parameters in equations (3) are based on those proposed in references [12] and [13].

$$\frac{\partial \boldsymbol{v}}{\partial t} + (\boldsymbol{v} \cdot \boldsymbol{\nabla})\boldsymbol{v} = -\boldsymbol{\nabla}\breve{P} + \nu\nabla^2\boldsymbol{v} - \psi\boldsymbol{\nabla}\frac{\delta\breve{\mathcal{F}}}{\delta\psi} \tag{1}$$

$$P = p + \frac{\delta\mathcal{F}}{\delta\psi} \tag{1a}$$

$$\boldsymbol{\nabla} \cdot \boldsymbol{v} = 0 \tag{1b}$$

$$\frac{\partial \psi}{\partial t} + (\boldsymbol{v} \cdot \boldsymbol{\nabla})\psi = M\nabla^2\frac{\delta\tilde{\mathcal{F}}}{\delta\psi} + \eta \tag{2}$$

$$\mu = \frac{\delta\mathcal{F}}{\delta\psi} = \rho_{ref}\,k_B T\left[\psi(r) - \frac{\psi(r)^2}{2} + \frac{\psi(r)^3}{3} - \int dr'\, C^{(2)}(|r-r'|)\psi(r')\right] \tag{3}$$

$$\hat{C}^{(2)}(k) = \sum_i \exp\left(-\frac{\sigma^2 k_i^2}{2\rho_i\beta_i}\right)\exp\left(-\frac{(k-k_i)^2}{2\alpha_i^2}\right) \tag{3a}$$

Table 1: Parameters for the HXPFC Equations

$\psi = \left(\frac{\rho(r)}{\rho_{ref}} - 1\right)$	Order parameter, representing density fluctuations
σ	Effective temperature
η	Optional Gaussian noise term that represents thermal fluctuations
ρ_{ref}	Reference liquid *number* density
M	Interface mobility
$\nu = \dfrac{\mu_{visc}}{m\rho_{ref}}$	Kinematic viscosity
m	Atomic mass
k_i	Interplanar spacing
ρ_i	Atomic density within specific plane
α_i	Controls interfacial properties
β_i	Number of planes in planar family
$\breve{P}, \breve{\mathcal{F}}$	Pressure and free energy respectively, normalized by $m\rho_{ref}$
$\tilde{\mathcal{F}}$	Dimensionless free energy, normalized by $\rho_{ref}k_B T$

2.2 Dimensionless Form of the HXPFC Equations

Equations (1)-(3) can be normalized to obtain the dimensionless groups. Equations (4)-(5) contain the dimensionless forms of equations (1)-(2) and Table 2 contains the resulting, novel parameter definitions. Furthermore, Table 2 presents the dimensionless group as numbered Pi terms, along with the name of their corresponding momentum or mass transfer analogies.

$$\frac{\partial \tilde{\boldsymbol{v}}}{\partial \tau} + (\tilde{\boldsymbol{v}} \cdot \tilde{\boldsymbol{\nabla}})\tilde{\boldsymbol{v}} = -\text{Eu}\,\tilde{\boldsymbol{\nabla}}\tilde{P} + \frac{1}{\text{Re}}\tilde{\nabla}^2\tilde{\boldsymbol{v}} - \Pi_3\psi\tilde{\boldsymbol{\nabla}}\frac{\delta\tilde{\mathcal{F}}}{\delta\psi} \tag{4}$$

$$\tilde{P} = \tilde{p} + \Pi_4\frac{\delta\tilde{\mathcal{F}}}{\delta\psi} \tag{4a}$$

$$\tilde{\boldsymbol{\nabla}} \cdot \tilde{\boldsymbol{v}} = 0 \tag{4b}$$

$$\frac{\partial \psi}{\partial \tau} + (\tilde{\boldsymbol{v}} \cdot \tilde{\boldsymbol{\nabla}})\psi = \frac{1}{\Pi_2}\tilde{\nabla}^2\frac{\delta\tilde{\mathcal{F}}}{\delta\psi} + \tilde{\eta} \tag{5}$$

Table 2: The complete dimensionless groups from dimensionless HXPFC equations.

$\Pi_1 = \dfrac{\nu}{M} = \dfrac{\text{Momentum Diffusivity}}{\text{Interface Diffusivity}}$	Analogous to Schmidt number
$\Pi_2 = \dfrac{v_0 L}{M} = \dfrac{\text{Advection}}{\text{Interface Diffusivity}}$	Analogous to Peclet number
$\Pi_3 = \dfrac{k_B T}{m v_0^2} = \dfrac{\text{Kinetic Energy Scaling}}{\text{Inertial Driving Force}}$	Analogous to Euler number
$\tau = \dfrac{v_0}{L} t = \dfrac{\text{Dimensional time}}{\text{Convective time}}$	Dimensionless timescale
$\Pi_4 = \dfrac{\rho_{ref} k_B T}{P_0}$	Result of normalized pressure

Note, equations (3) remain the same as previously defined and the Euler (Eu) and Reynolds (Re) numbers have their usual fluid mechanics definitions. Moreover, equations (3)-(5) will be the forms used to conduct numerical experiments in §3 to reveal interactions and dependencies between parameters without needing to know specific dimensional parameters. It may be noticed that after non-dimensionalizing equations (1)-(2), equations (4)-(5) are missing the Schmidt like number, Π_1. However, it may be recovered by dividing Π_2 by Re.

The form of Π_3 was presented and defined differently in reference [15]. Dimensionless group Π_3 was reported in reference [15] as the "Peclet" number. However, the parameter modulates the strength of the momentum coupling between the growing crystal and the fluid, not necessarily adhering to the traditional definition of the Pe number. It should also be mentioned, using intuition from the driving force of nucleation and classical nucleation theory (CNT), a phenomenologically modified representation of the Π_3 dimensionless group can be obtained. Instead, Π_3 can be phenomenologically modified by replacing $k_B T$ with the critical Gibbs Free energy, ΔG^*, to gain better insight into the competing forces during homogenous nucleation. Furthermore, considering, $\Delta G^* \propto k_B T$, corresponds to the chemical potential difference between the solid and liquid phases prior to complete crystallization, the simple modification is not a far stretch from reality. In addition, the parameter, Π_3, appears to have more significance in flow-mediated crystallization than previously understood because it can now be thought of as the ratio of crystallization driving force to advection. As the PFC here only demonstrates a toy model, the modified Π_3 parameter cannot be estimated from typical CNT parameters. A future study will require a more quantitative subscale model to fully parameterize the energetic driving forces for crystallization.

3 NUMERICAL METHODS AND SIMULATIONS

Equations (3)-(5) were used for the simulations, to study the effects of dimensionless parameters, Π_2, Π_3, Re, and implicitly Π_1, on the crystal growth kinetics. If equations (3)-(5) are solved pseudo-spectrally using periodic boundary conditions (PBC), the convolution becomes multiplication in frequency space. Furthermore, most PFC studies are performed using pseudo-spectral methods as they are computationally efficient, relatively easy to implement, and implicitly satisfy periodic boundary conditions. However, because we are interested in Couette-type flow to imitate thin-film flows, periodic boundary conditions in all directions are

no-longer acceptable. Hence, to solve equations (3)-(5) without PBCs, there are a few alternatives. If pseudo-spectral methods are desired, Chebyshev polynomials must be used in the non-periodic direction. Alternatively, non-spectral methods can be used, i.e. Finite Difference (FDM), Finite Element (FEM), or Finite Volume (FVM) methods. However, all methods have in common the challenge of solving the convolution operation in equation (3) with Neumann boundary conditions (NBC).

3.1 XPFC with Neumann Boundary Conditions

To solve the convolution with boundary conditions in equation (3), in two dimensions, the simulation domain is mirrored over one of the non-periodic dimensions and translated over one of the periodic dimensions, inspired by the Chebyshev spectral differentiation by Fast Fourier Transform (FFT) algorithm in reference [18]. Furthermore, the positive wavenumbers used to calculate the DCF in equation (3a) now range from 1 to M_i, instead of $M_{i/2}$ where M_i is the number of grid points in dimension i. Then the two functions are multiplied in Fourier space, following the convolution theorem. Note, only the first M_i rows and columns are kept from the extended domain. Unfortunately, solving the non-periodic convolution using the mirrored approach increases the computational cost (number of total grid points) by a factor of 4.

To verify the implementation of Neumann boundary conditions for solving XPFC during crystal growth, equation (2) is solved using the same DCF parameters reported in reference [21], by directly comparing the effects of the convolution. Equations (2) and (3) are solved with and without full PBCs, using a simple second order in space finite difference scheme. The convolution with full PBCs can be treated simply using the standard convolution theorem, whereas the convolution with PBCs and NBCs is solved using the mirroring approach. We observed that the crystal growth remains largely unaffected by the mirrored convolution until the crystal reaches the edge of the computational domain. The edge effects on crystal growth can be nonetheless reduced by using a larger simulation box to gain a prolonged study of the unaffected crystal growth.

3.2 HXPFC with Neumann Boundary Conditions

The modified Navier-Stokes equations (4) were solved using a projection method on a typical staggered grid[19], with the velocities solved on cell faces, and the pressure solved in cell centers. The staggered grid was selected to avoid instabilities found when solving equations (3)-(5) on a collocated grid. Furthermore, the pressure Poisson equation was solved using a modified Gauss-Seidel method[20]. The minor modification allowed for one dimension to be vectorized, speeding up convergence. In addition, a simple second-order in space finite difference scheme was used to solve equations (5) on the cell vertices. Equation (5) was solved first and used to obtain $\frac{\delta \mathcal{F}}{\delta \psi}$ at the next timestep. Then, the next time step chemical potential was inserted into equation (4) and only included in the non-divergence free update of the projection method. Refer to Table 3 for more details. Note, all time-steps were discretized using forward Euler step.

Table 3: Steps to solving the Dimensionless HXPFC equations

Prescribe initial conditions

	Define grid-points and wave numbers, calculate DCF
1	Calculate convolution at current time step in equation (3)
2	Use convolution in step 1 to calculate equation (3) at current time step
3	Use equation (3) and velocities at current time step to calculate equation (5) at next time step
4	Use equation (5) at next time step to calculate viscous update in equation (4)
5	Proceed with standard Navier-Stokes Projection method[19]
6	Repeat steps (1)-(5)

3.3 Simulation Setup

To analyze the effects of each dimensionless number in a simple shear flow, three different simulations were performed with specific combinations of dimensionless numbers, listed in Table 4. The Euler number was set to unity for all simulations. Furthermore, each combination of dimensionless parameters was not random. For instance, the Π_2 simulations were tested in laminar flow, while limiting the contribution from Π_3. It was chosen as the first of the simulations because Π_2 presumably had the largest effect on crystal growth. In addition, the Π_3 simulations were selected based on $\Pi_2=20$ being the best balance of crystal growth and advection. Furthermore, the range of Π_3 was chosen to identify the momentum coupling strength effects. Lastly, because Re and Π_3 appear in equation (4), it was reasonable to assume there are interactions between the parameters. Hence, the Π_3 simulations results were used to identify the most dramatic Π_3 term, and Re was intentionally selected in an attempt to modify the effects of Π_3.

Table 4. Dimensionless parameter combinations for simulations

Simulation	Re	Π_2	Π_3
Π_2 Simulations	100	5-80	1
Π_3 Simulations	100	20	10-1500
Re - Π_3 Simulations	5-1500	20	1500

To eliminate the transient behavior from the flow field, the fully developed, analytical solution to simple shear flow was used as the initial condition for equation (4). The only fluctuations in the flow field were due to crystal growth and the effect of specific dimensionless parameters. Equations (6) and (7) prescribe the initial conditions for the order parameters[13,21].

$$\psi_{sq} = A_{10}\left(\left(3\sqrt{2}-2\right)\cos\left(2\pi y/a_{sq}\right) - 2\cos\left(2\pi x/a_{sq}\right)\right) \\ - A_{11}\cos\left(2\pi x/a_{sq}\right)\cos\left(2\pi y/a_{sq}\right) + \psi_0 \tag{6}$$

$$\psi_{tri} = A(\cos(2\pi x/a_{tri})/2 + \cos(\pi x/a_{tri})\cos(\sqrt{3}\pi y/a_{tri}) + \psi_0 \tag{7}$$

Equation (6) is the two-mode approximation to the square phase and equation (7) is the one-mode approximation for the triangular (hexagonal) phase. However, in the following simulations, equation (7) is used exclusively to form the initial seed because ψ_0 and σ were selected to place the system in the triangular phase. Furthermore, to obtain the initial crystal

seed, the order parameter is multiplied by a gaussian, centered at the center particle. Additionally, the width of the gaussian is modified to retain seven particles in the initial seed. The seven particle initial seed is then grown to completion, i.e. when the entire domain is crystallized.

PBCs are used in streamwise directions in equations (4) - (4b), including the pressure Poisson equation. However, in equation (4), one of the spanwise directions has a moving wall boundary condition, and the other a zero Dirichlet boundary condition. Alternatively, in the spanwise direction of the pressure Poisson equation, Neumann boundary conditions are used. Additionally, PBCs and NBCs are used in the streamwise and spanwise directions, respectively, of equation (5). Note, the moving wall boundary condition is set to unity in equation (4).

4 RESULTS AND DISCUSSION

The parameter tests were all performed on a $(x, y) \in \Omega = [0,1] \times [0,1]$ domain using $N = 512$ grid points and $Lx = 64$ used for the length scale of the crystal. Additionally, the parameters, ψ_0 and σ, for equations (3), (5), and (7) were set to 0.06 and 0.12, respectively, placing the stable equilibrium structure in the triangular/hexagonal phase[21]. Furthermore, the length-scale means controlling the number and relative size of particles in the density field, i.e. increasing the length scale, increases the number of particles, and decreases the relative size of particles to the normalized domain. Additionally, the number of particles were calculated using a modified algorithm from references [22] and [23].

4.1 Π_2 (Peclet-like Number) Simulations

The Π_2 simulations were tested according to the parameter combinations in Table 3. Furthermore, the influence of Π_2 was studied first because in dimensionless form, it takes the place of mobility, and presumably has the largest impact on crystal growth. Figure 1 shows the test results.
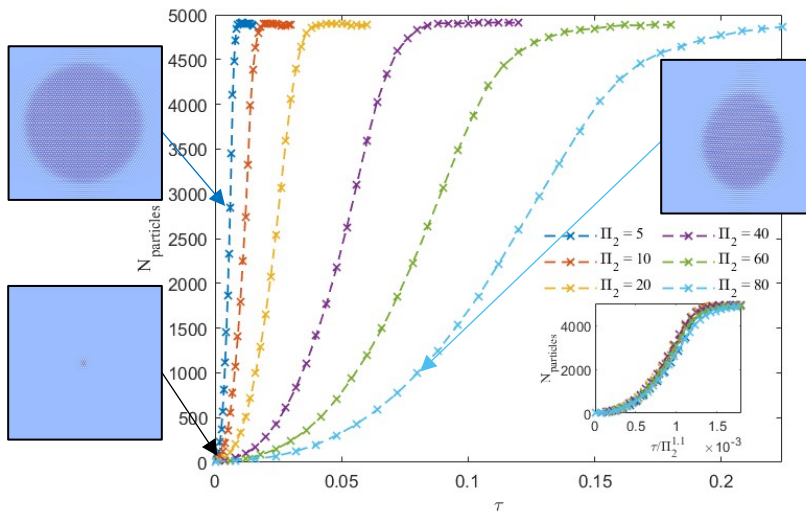

Figure 1: Results from varying the 'Peclet' like parameter, Π_2, showing increased advection stymies crystal growth. Furthermore, the inset images give more information on crystal structure at dimensionless timestep $\tau/\Pi_2 = 1\text{E}^{-3}$. Note, the arrow color corresponds to the legend, and the initial condition applies to all Π_2.

The main takeaway from Figure 1 is that increasing flow hinders crystal growth, which agrees with previous attempts using the hydrodynamic phase field crystal models[15-17]. Moreover, referring to the upper insets, the shear flow also dictates the shape of the crystal, as the crystal front changes with respect to the flow strength. Alternatively, the timescale in the lower inset of Figure 1 was divided by each respective Π_2 parameter and raised to the exponent of 1.1, resulting in a collapse of the curves. The slight super-linear dependence on $1/\Pi_2$ (as opposed to linear dependence) reveals an enhanced suppression effect on crystal growth with increasing Π_2 due to the presence of wall. If only the central regions (away from the wall) are considered for the growth, the normalized curves were found to collapse with a perfect exponent of 1.0 (not plotted).

4.2 Π_3 (Euler-like Number) Simulations

After identifying the Π_2 parameter dynamics, parameter combinations were better selected for the Eu-like Π_3 tests. A range spanning three orders of magnitude were chosen for Π_3 to detect the influence of competition of crystallization driving force and flow inertia. Figure 2 contains the effects of Π_3 on the growth of crystal, quantified by the number of density peaks.
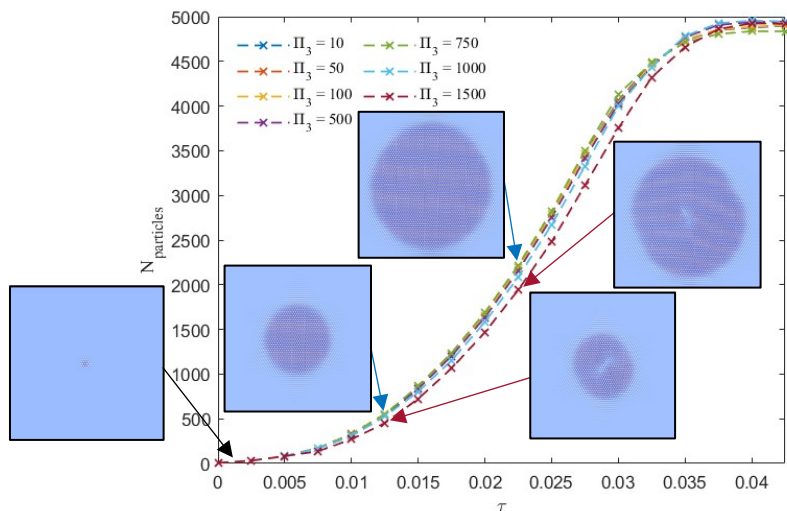

Figure 2: Results from varying the 'Eu' like number, Π_3. The curves indicate nothing about the crystal structure, rather the insets show the true effect of Π_3. Note, the arrow color corresponds to the legend, and the initial condition applies to all Π_3.

While the particle curves in Figure 2 indicate negligible dependence of the number of particles during crystal growth on Π_3, the insets show Π_3 affects the local crystal structure, especially at the crystal seed region and the growth fronts. Furthermore, the local transformation of crystal microstructure is accompanied by a local fluctuation of fluid velocity like a Marangoni flow effect[24]. Nonetheless, more studies will be required to further elucidate the effect of the Π_3 term for controlling crystal growth.

4.3 Re - Π_3 Simulations

Since Re and Π_3 both appear in equation (4), the parameters should have interactions affecting both crystal growth and the corresponding flow field. The range of Re was selected to show either suppression or enhancement of the effects of Π_3 (the local crystal structural transformation through a Marangoni-like effect). The simulations were run according to the parameters in Table 4. Figure 3 contains the number of particles versus time for various Re.
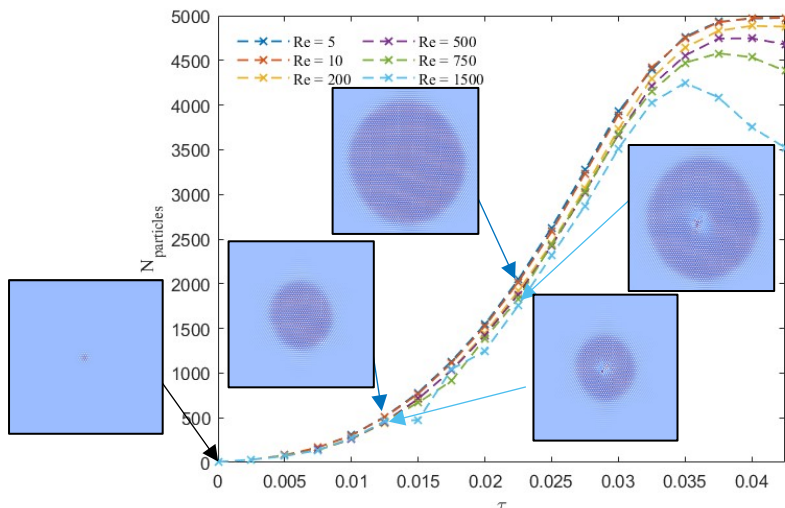

Figure 3: Results from varying Re, with $\Pi_3 = 1500$. The curves show negligible dependence of number of particles during early time crystal growth on Re, rather the insets show decreasing and increasing Re suppresses and enhances the Marangoni-like effect, respectively. At late times and increasing Re shows internal melting from enhanced Marangoni-like effect. Note, the arrow color corresponds to the legend, and the initial condition applies to all Re.

Interestingly, it was again found that the momentum parameter, Re, does not have a significant impact on the number of particles during early time crystal growth. However, at late times and increasing Re, the Π_3 induced, Marangoni-like flow causes slight internal melting. Additionally, Re can either suppress (with low Re number) or enhance (with high Re number) the effects of Π_3, depending on the Reynold number selected. The intricate dynamics of Re and Π_3 reveal the importance of selecting proper solvent and flow regime (e.g., laminar vs turbulence) on crystal microstructural transformation. Since thin-film flows are primarily in the laminar regime based on length scale and geometric arguments, the flow regime may have lesser importance than selecting solvent properties (viscosity and surface tension).

4.4 Microstructural Transformations

In addition to studying parameter effects on crystal growth, the effect of Π_2 on crystal structural transformations was also investigated. The structural transformations were performed on a $(x, y) \in \Omega = [0,1] \times [0,1]$ domain using $N = 256$ grid points and $Lx = 32$ used for the length scale of the crystal. Furthermore, the parameters, ψ_0 and σ, for equations (3), (5), and (7) were set to 0.06 and 0.10, respectively, again placing the stable equilibrium structure in the triangular/hexagonal phase[21]. The temperature like parameter, σ, was set closer to the

9

triangular/square coexistence line to promote transition. In addition, the flow remained in simple shear flow, and the parameter combinations followed those used for the Π_2 simulations, Table 4. Figure 4 contains a few snapshots from the structural phase transition tests.
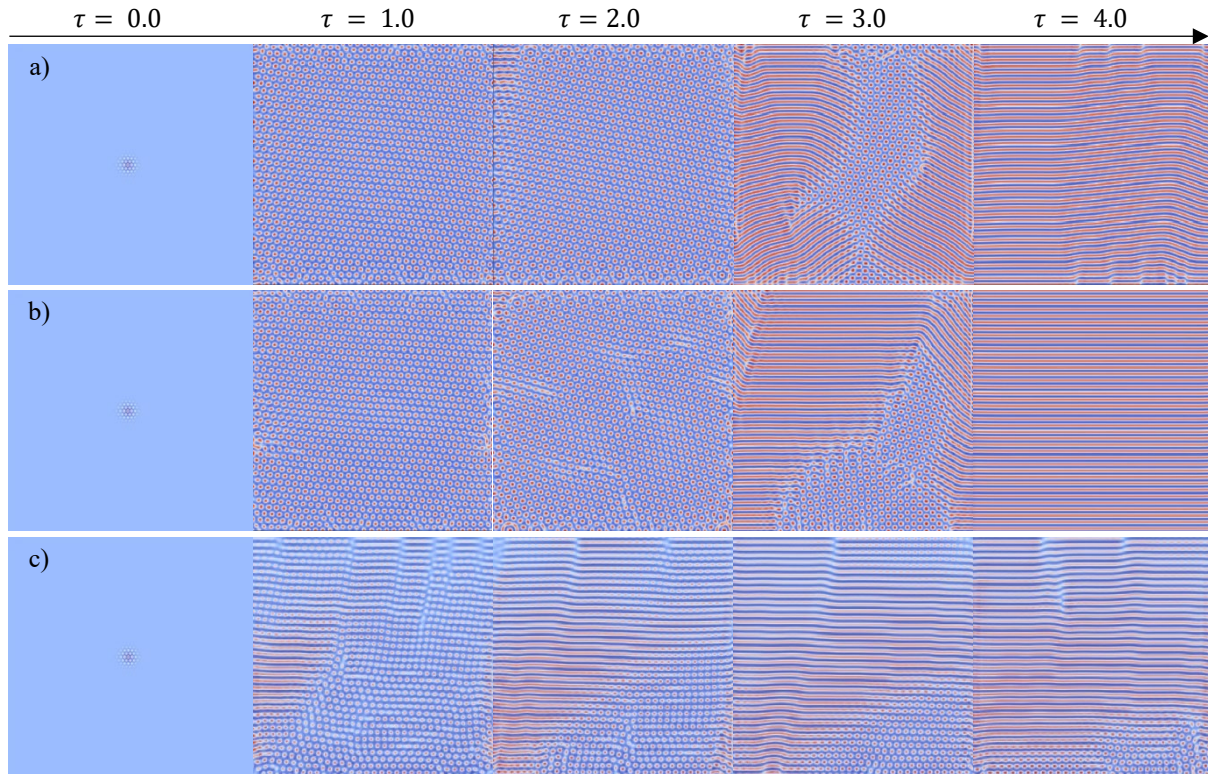

Figure 4: Snapshots of crystal transformation from hexagonal to striped phase at increasing points in time. **a)** $\Pi_2 = 5$ **b)** $\Pi_2 = 10$ **c)** $\Pi_2 = 80$

Figure 4 shows that at the long-time regime, the advection can push the triangular/hexagonal phase into a striped phase, often seen in soft matter. It is worth noting that Greenwood et al. reported[13] the XPFC without flow effect was unable to give rise to a stable striped phase. Here, we demonstrate that advection appears to promote a stable equilibrium striped phase. Furthermore, when $\Pi_2 = 80$, the structural transformation from triangular to square phase occurs prior to transitioning into the striped phase. The time to eventually transitioning to a striped phase seems to be further dependent on the Peclet-like number Π_2. The current study of flow-mediated crystal phase transition (due to Peclet-like number Π_2) points towards intriguing spatiotemporal control strategies of crystal phases using the simple shear flow, where further studies are warranted to comprehensively map out the phase diagram with the addition of the flow effect axis.

5 CONCLUSIONS

We demonstrate the promise of the HXPFC modeling crystallization in the presence of flow. It was shown that there is important interplay between Π_2, Π_3, and Re on crystal growth and structural transformation. It was also shown that Π_2 has most influence on kinetics of crystal

growth as well as the long-time equilibrium structure, while Π_3 and Re synergistically can alter the local crystal structure through a Marangoni-like flow effect. Additionally, the effects of Π_3 and Re also highlight the importance of solvent selection. While the HXPFC has promise for modelling crystallization in flow, there is still much work to be done. Common with all PFC models, calibration is needed to connect the PFC to a specific material. With direct access to the DCF, and structure factor, the model may be parameterized via molecular dynamics simulations[25] or possibly experimental images such as TEM/SEM images. Other phenomena such as nucleation, crystal Brownian motion, etc., can be further incorporated to refine the validity of the model. Of note, the previous phenomena require physically accurate noise, which is another common challenge to all PFC models. Nonetheless, the current model demonstrates potential in capturing rich physics regarding flow-mediated crystallization owing to its accessibility to mesoscopic length and (diffusive) time scales, and direct free energy and chemical potential access.

REFERENCES

[1] Zheng D, Raffin F, Volovitch P, Pauporté T. Control of perovskite film crystallization and growth direction to target homogeneous monolithic structures. *Nat Commun.* (2022) 13(1):6655.

[2] Wei Chou K, Ullah Khan H, Niazi MR, Yan B, Li R, Payne MM, et al. Late stage crystallization and healing during spin-coating enhance carrier transport in small-molecule organic semiconductors. *J Mater Chem C.* (2014) 2(28):5681–9.

[3] Chen LY, Liang SX, Liu Y, Zhang LC. Additive manufacturing of metallic lattice structures: Unconstrained design, accurate fabrication, fascinated performances, and challenges. *Materials Science and Engineering: R: Reports.* (2021) 146:100648.

[4] Ramakrishnan TV, Yussouff M. First-principles order-parameter theory of freezing. *Phys Rev B.* (1979) 19(5):2775–94.

[5] Marconi UMB, Tarazona P. Dynamic density functional theory of fluids. *The Journal of Chemical Physics.* (1999) 110(16):8032–44.

[6] Elder KR, Katakowski M, Haataja M, Grant M. Modeling Elasticity in Crystal Growth. *Phys Rev Lett.* (2002) 88(24):245701.

[7] Elder KR, Grant M. Modeling elastic and plastic deformations in nonequilibrium processing using phase field crystals. *Phys Rev E.* (2004) 70(5):051605.

[8] Emmerich H, Löwen H, Wittkowski R, Gruhn T, Tóth GI, Tegze G, et al. Phase-field-crystal models for condensed matter dynamics on atomic length and diffusive time scales: an overview. *Advances in Physics.* (2012) 61(6):665–743.

[9] Berry J, Provatas N, Rottler J, Sinclair CW. Phase field crystal modeling as a unified atomistic approach to defect dynamics. *Phys Rev B.* (2014) 89(21):214117.

[10] Shen HF, Peng Q, Wu WP. Phase field crystal study on the size and strain rate dependent evolution of Kirkendall voids in binary alloy. *Journal of Alloys and Compounds.* (2024) 983:173832.

[11] Alster E, Montiel D, Thornton K, Voorhees PW. Simulating complex crystal structures using the phase-field crystal model. *Phys Rev Materials.* (2017) 1(6):060801.

[12] Greenwood M, Provatas N, Rottler J. Free Energy Functionals for Efficient Phase Field Crystal Modeling of Structural Phase Transformations. *Phys Rev Lett.* (2010) 105(4):045702.

[13] Greenwood M, Rottler J, Provatas N. Phase-field-crystal methodology for modeling of structural transformations. *Phys Rev E.* (2011) 83(3):031601.

[14] Praetorius S, Voigt A. A Phase Field Crystal Approach for Particles in a Flowing Solvent. *Macromolecular Theory and Simulations.* (2011) 20(7):541–7.

[15] Praetorius S, Voigt A. A Navier-Stokes phase-field crystal model for colloidal suspensions. *The Journal of Chemical Physics.* (2015) 142(15):154904.

[16] An J, Zhang J, Yang X. A novel second-order time accurate fully discrete finite element scheme with decoupling structure for the hydrodynamically-coupled phase field crystal model. *Computers & Mathematics with Applications.* (2022) 113:70–85.

[17] Yang J, Kim J. Consistent energy-stable method for the hydrodynamics coupled PFC model. *International Journal of Mechanical Sciences.* (2023) 241:107952.

[18] Trefethen LN. *Spectral methods in MATLAB.* Society for Industrial and Applied Mathematics, Vol. I, (2000).

[19] Fletcher CAJ. *Computational Techniques for Fluid Dynamics 2: Specific Techniques for Different Flow Categories.* Springer Berlin Heidelberg, Vol. I, (1991).

[20] Strikwerda JC. *Finite difference schemes and partial differential equations.* Society for Industrial and Applied Mathematics, Vol. I, (1989), Vol. II, (2004).

[21] Huang Y, Wang J, Wang Z, Li J, Guo C, Guo Y, et al. Existence and forming mechanism of metastable phase in crystallization. *Computational Materials Science.* (2016) 122:167–76.

[22] Crocker JC, Grier DG. Methods of Digital Video Microscopy for Colloidal Studies. *Journal of Colloid and Interface Science.* (1996) 179(1):298–310.

[23] Tikuišis, K. (2024). peaks2 - find peaks in 2D data without additional toolbox (https://www.mathworks.com/matlabcentral/fileexchange/113225-peaks2-find-peaks-in-2d-data-without-additional-toolbox), MATLAB Central File Exchange.

[24] Gouiller C, Ybert C, Cottin-Bizonne C, Raynal F, Bourgoin M, Volk R. Two-dimensional numerical model of Marangoni surfers: From single swimmer to crystallization. *Phys Rev E.* (2021) 104(6):064608.

[25] Asadi E, Asle Zaeem M, Nouranian S, Baskes MI. Quantitative modeling of the equilibration of two-phase solid-liquid Fe by atomistic simulations on diffusive time scales. *Phys Rev B.* (2015) 91(2):024105.